Electronic supplementary information

Self-supported mesoscopic tin oxide nanofilms for electrocatalytic reduction of carbon dioxide to formate

Juwon Jeong,‡[ab] Jin Soo Kang,‡[abc], Heejong Shin,[ab] Soo Hong Lee,[ab] Junghwan Jang,[ab] Taeghwan Hyeon,[ab] Hyun S. Park*[d] and Yung-Eun Sung*[ab]

[a]Center for Nanoparticle Research, Institute for Basic Science (IBS), Seoul 08826, Republic of Korea.

[b]School of Chemical and Biological Engineering, Seoul National University, Seoul 08826, Republic of Korea.

[c]Department of Chemical Engineering, Massachusetts Institute of Technology, Cambridge, MA 02139, USA.

[d]Center for Hydrogen·Fuel Cell Research, Korea Institute of Science and Technology (KIST), Seoul 02792, Republic of Korea

‡These authors contributed equally to this work.

*Corresponding authors. E-mail: hspark@kist.re.kr (H. S. Park), ysung@snu.ac.kr (Y.-E. Sung)

Experimental

Preparation and characterization of nanostructured SnO_2 electrodes

Anodization of Sn foil (Alfa Aesar, 0.25 mm-thick, 99.8%) was carried out in 0.5 M oxalic acid in a two-electrode system (with the assistance of ultrasonication), where a Pt wire was used as counter electrode. The distance between the two electrodes was 5 cm, and 10 V was applied for 10 min. As-anodized electrode was washed with distilled water and was dried in an oven, followed by theraml annealing in air at 500 °C for 3 h. The morphology of SnO_2 electrodes were examined by SEM using Carl Zeiss MERLIN Compact, and XRD patterns were collected by using Rigaku D-MAX2500-PC. XPS analyses were carried out using a synchrotron radiation source at 10A2 beamline of Pohang Accelerator Laboratory (PAL) or by using Thermo Sigma Probe equipped with an Al-Kα source. XAFS measurements were performed at 10C beamline of PAL, and the data were processed by using Demeter software package. A potentiostat (Autolab PGSTAT302N) was used for the estimation of EDLCs.

Electrochemical reduction of CO_2

For CO_2RR, all electrochemical measurements were carried out in a three-electrode configuration using a homemade gas-tight H-type cell and Autolab PGSTAT302N, with a Ag/AgCl reference electrode (filled with saturated KCl solution) and a graphite rod counter electrode. The glass cell was comprised of anodic and cathodic compartments which were separated by cation exchange membrane (Nafion®117) to prevent any contamination by crossovers between cathode and anode. Ohmic resistance of solution was measured using electrochemical impedance spectroscopy (EIS) before the reaction and was used for iR correction for all of the measurements. CO_2-saturated 0.5 M $KHCO_3$ was used as electrolyte; CO_2 gas was delivered with specific rate (20 sccm) from at least 30 minutes before the reaction and was continuously purged throughout the measurements. In the case of steady-state CO_2RR, cathodic electrolyte was continuously stirred at 400 rpm. All potentials were converted to RHE scale by using the following equation:

$$E_{RHE} = E_{Ag/AgCl} + 0.197\ V + 0.0592\ pH \quad (1)$$

Analyses of products from CO_2RR

Gaseous products were analyzed by using a GC (Agilent 7890B) equipped with a flame ionization detector (FID) and a thermal conductivity detector (TCD) for detection of CO and H_2, respectively. FE of each gaseous product was calculated from the obtained volume concentration using the following equation:

$$FE_j = \frac{i_j}{i_{total}} \times 100\% = \frac{2 \times F \times \frac{p_0 Q v_j}{RT}}{i_{total}} \times 100\% \ (j = H_2 \ or \ CO) \qquad (2)$$

(2)

(where v_j = volume concentration measured from GC, Q = flow rate of delivering CO_2, F = 96485 C mol^{-1}, p_0 = 101325 Pa, R = 8.314 J mol^{-1} K^{-1}, T = 298.15 K, and i_{total} = overall current measured at the moment of injection). The detailed derivation processes of the equation (2) is presented in the Supporting Information. Quantification of formate was performed by measuring 600 MHz NMR peak area using Bruker AVANCE 600. The sample for ^{1}H NMR was prepared by mixing 450 μL aliquot of electrolyte with 50 μL of 1% 3-(trimethylsilyl)-1-propanesulfonic acid (DSS) in D_2O (Sigma-Aldrich). The formate peak area on ^{1}H NMR (δ = 8.445) was converted to the amount of formate based on the calibration curve in Fig. S8. Then, formate selectivity was calculated by dividing this amount by the total charge consumed during the CO_2RR. All of the experiments related to product quantification were conducted at least three times to verify the reliability of our results by presenting the statistics.

Calculation of Faradaic efficiencies of gaseous products

In general, Faradaic efficiency (FE) is calculated by dividing the charges used for producing a specific product by the overall charges that flowed. For the CO_2RR in this study, GC signal collected at the moment of injection was used for the evaluation of FE, which can be summarized as the following equation:

$$FE_j = \frac{i_j}{i_{total}} \times 100\% \ (j = each\ product) \quad (1) \tag{3}$$

i_{total} can be obtained from the experimental data, and i_j could be calculated from the equations written below. From the definition of current, i_j can be expressed as follows:

$$i_j = \frac{dC_j}{dt} \quad (2) \tag{4}$$

Then, using the product-charge relationship and ideal gas equation (pV = nRT), the charge C_j could be written as Eqn. 5.

$$C_j = mFn_j = mF\frac{p_0 V_j}{RT} \quad (3) \tag{5}$$

Since the flow rate is a fixed value, V_j can be expressed by using the signal obtained from GC, as follows:

$$\frac{dV_j}{dt} = v_j Q \quad (4) \tag{6}$$

By combining the three equations (Eqns. 4-6) and substituting *m* with 2 for the cases of H_2 and CO productions, i_j can be rearranged as Eqn. 7.

$$i_j = 2 \times F \times \frac{p_0 v_j Q}{RT} \quad (5) \tag{7}$$

Finally, equation for FE can be derived by Eqns. 3 and 7. The following equation is also shown as Eqn. 2 above.

$$FE_j = \frac{2 \times F \times \frac{p_0 Q v_j}{RT}}{i_{total}} \times 100\% \tag{8}$$

Abbreviations

C_j = total charge used to produce the product j [=] C

m = the number of electrons used to produce a molecule j

n_j = the total mole number of product j [=] mol

V_j = the total volume of product j [=] m^3

v_j = the volume percentage of product j measured from GC signal

Q = total flow rate [=] $m^3\ s^{-1}$

(j = H_2 or CO)

Table S1. Summary of fitted results from XPS O 1s spectra displayed in Fig. 2b.

Electrodes		Lattice Oxygen	Non-Stoichiometric Oxygen	Adsorbed Species
Sn foil	Peak Positions	530.34 eV	532.01 eV	533.39 eV
	Areal Ratio	40.47 %	48.64%	10.89%
AN-SnO_x	Peak Positions	530.47 eV	531.79 eV	-
	Areal Ratio	50.77%	49.23%	-
TA-SnO_2	Peak Positions	530.75 eV	531.78 eV	-
	Areal Ratio	54.77%	45.23%	-

Table S2. Comparisons on electrochemical CO_2RR performances of TA-SnO_2 and previously reported formate-producing Sn-based catalysts.

Electrode Materials	**Electrolyte**	**Potential (V vs. RHE)**	**$FE_{formate}$ (%)**	**j_{HCOO^-} (mA/cm^2)**	**References (year)**
TA-SnO_2	0.5 M $KHCO_3$	–0.80	60.11	33.66	This work
Surface-engineered Sn foil	0.1 M $KHCO_3$	–1.09	77.4	3.7	S1 (2017)
Sn dendrite/Sn foil	0.1 M $KHCO_3$	–1.36	71.6	~23	S2 (2015)
Sn-Cu alloy	0.1 M $KHCO_3$	–0.50	95	31.4	S3 (2019)
Ag-Sn core-shell alloy	0.5 M $NaHCO_3$	–0.90	87.2	~25	S4 (2017)
Sn quantum sheet/graphene	0.1 M $NaHCO_3$	–1.13	89	18.7	S5 (2016)
Sn/SnO_x thin film	0.5 M $NaHCO_3$	–0.7	~40	~1.6	S6 (2012)
SnS_2-derived Sn/ reduced graphene oxide	0.1 M $KHCO_3$	–1.05	90	10.0	S7 (2017)
SnO_2 nanoparticles/ carbon cloth	0.5 M $NaHCO_3$	–1.07	85	45	S8 (2017)
Sn(S)/Au needle	0.1 M $KHCO_3$	–0.75	95	51.2	S9 (2017)

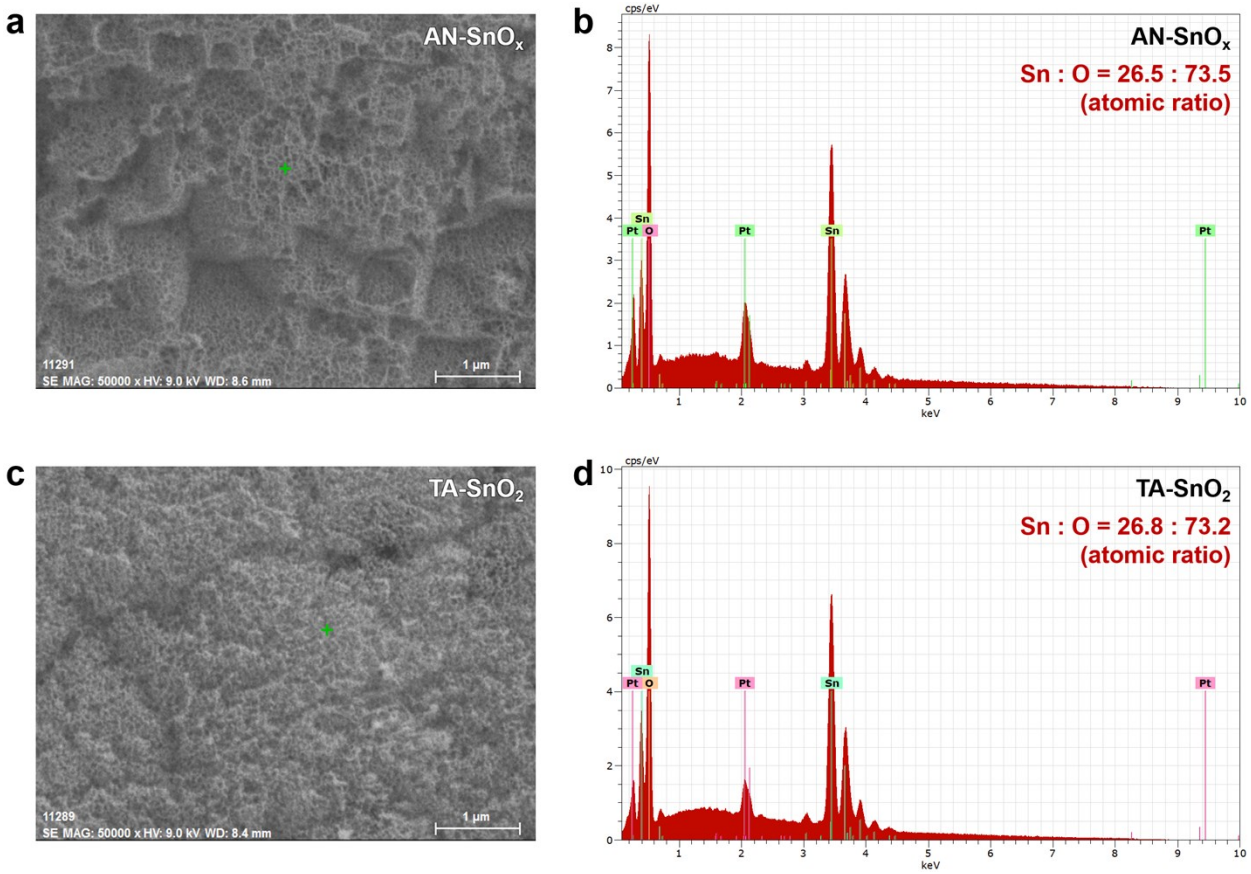

Fig. S1. (a) SEM image of AN-SnO_x and (b) corresponding EDS spectrum. (c) SEM image of TA-SnO_2 and (d) corresponding EDS spectrum. For assigning the EDS signals, Pt was included in addition to Sn and O due to the presence of thin layer of Pt deposited on the surface to improve the conductivity during the SEM analysis.

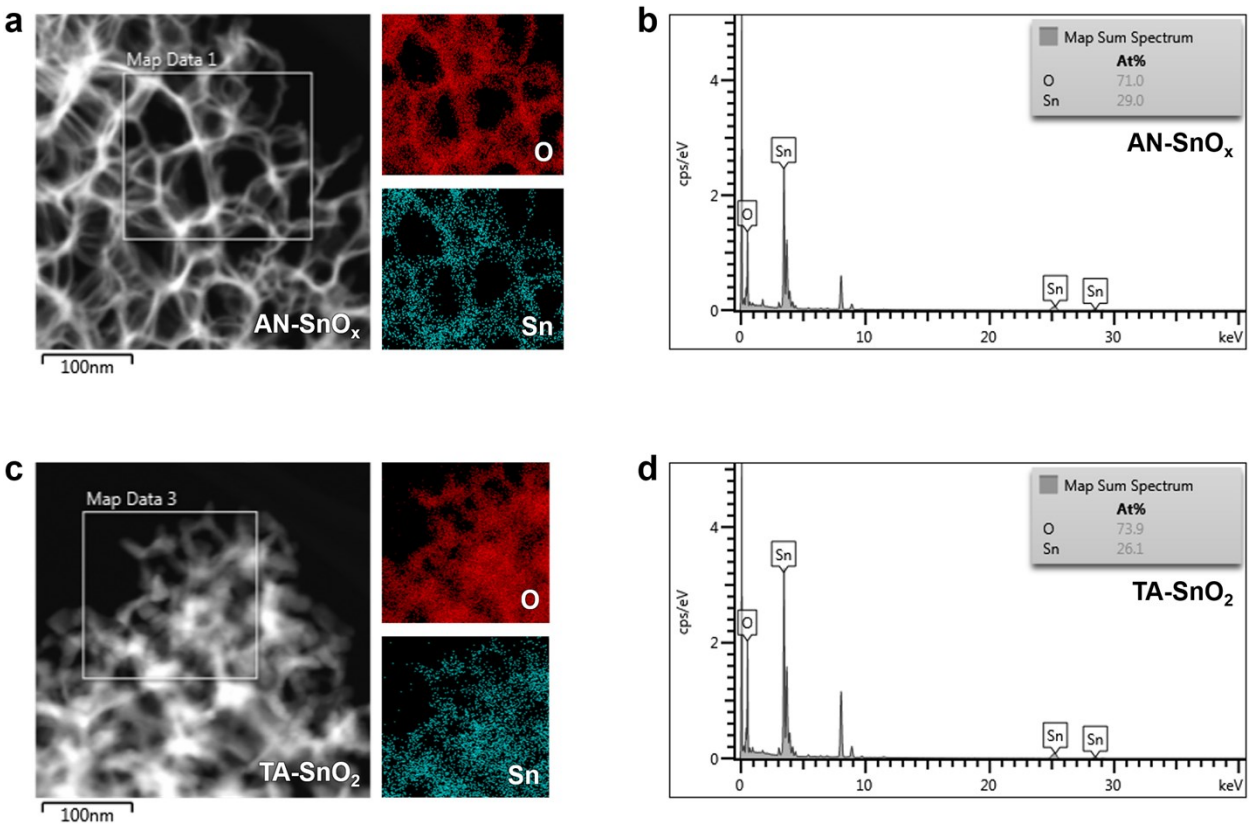

Fig. S2. (a,c) Scanning transmission electron microscopy (STEM) image of (a) AN-SnO_x and (c) TA-SnO_2 and corresponding elemental maps of O and Sn. (b,d) EDS spectra (b) AN-SnO_x and (d) TA-SnO_2 obtained from the regions marked in (a) and (c), respectively.

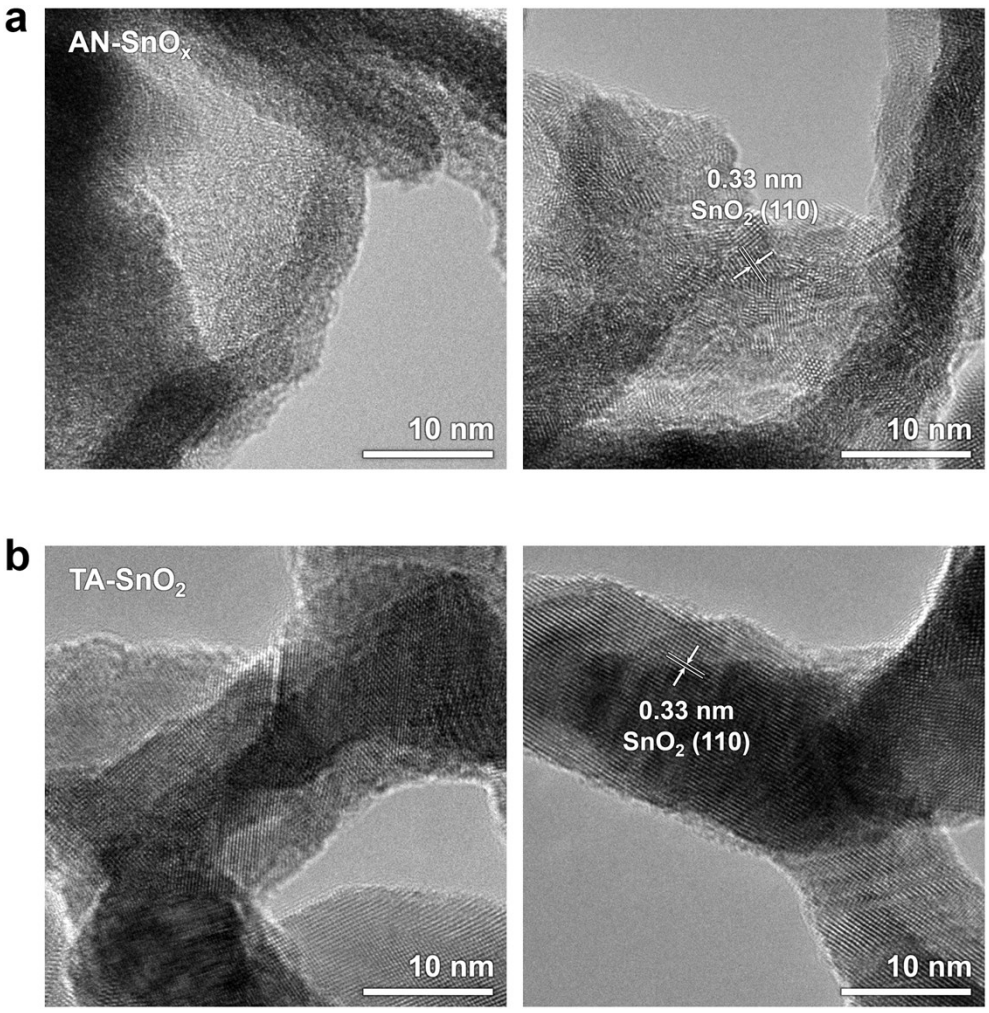

Fig. S3. High-magnification TEM images of (a) AN-SnO_x and (b) TA-SnO_2.

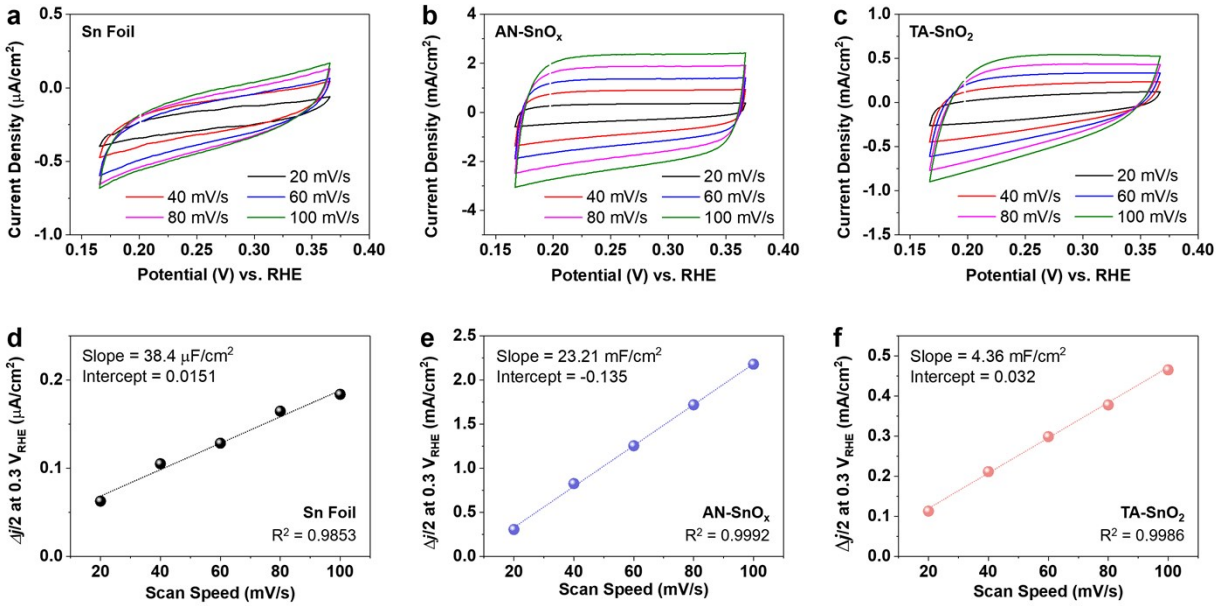

Fig. S4. (a-c) CV diagrams of (a) Sn foil, (b) AN-SnO_x, and (c) TA-SnO_2 measured in Ar-saturated 0.5 M $KHCO_3$ electrolyte at various scan rates. The potential window of 0.17 to 0.37 V was selected to minimize possible interference from Sn-oxidation and SnO_x-reduction currents. (d-f) Capacitive currents respectively obtained from (a-c) at 0.3 V and their linear fits for calculations of EDLCs of (d) Sn foil, (e) AN-SnO_x, and (f) TA-SnO_2.

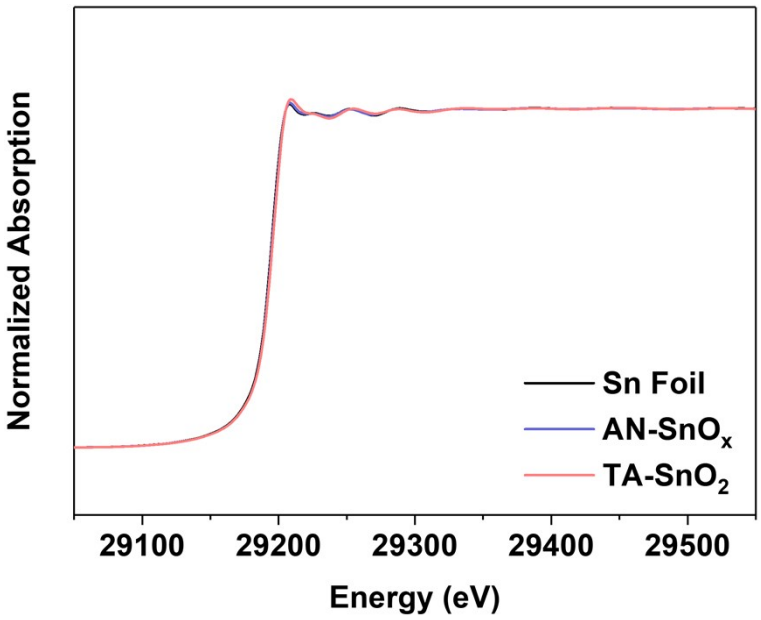

Fig. S5. XAFS spectra of Sn foil, AN-SnO_x, and TA-SnO_2.

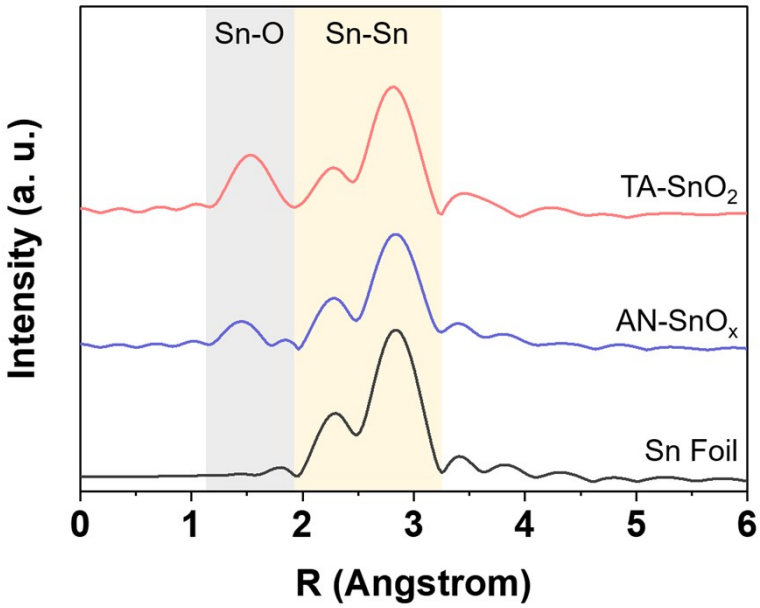

Fig. S6. k^3-weighted Fourier transform of EXAFS spectra of Sn foil, AN-SnO_x, and TA-SnO_2 obtained at Sn K-edge.

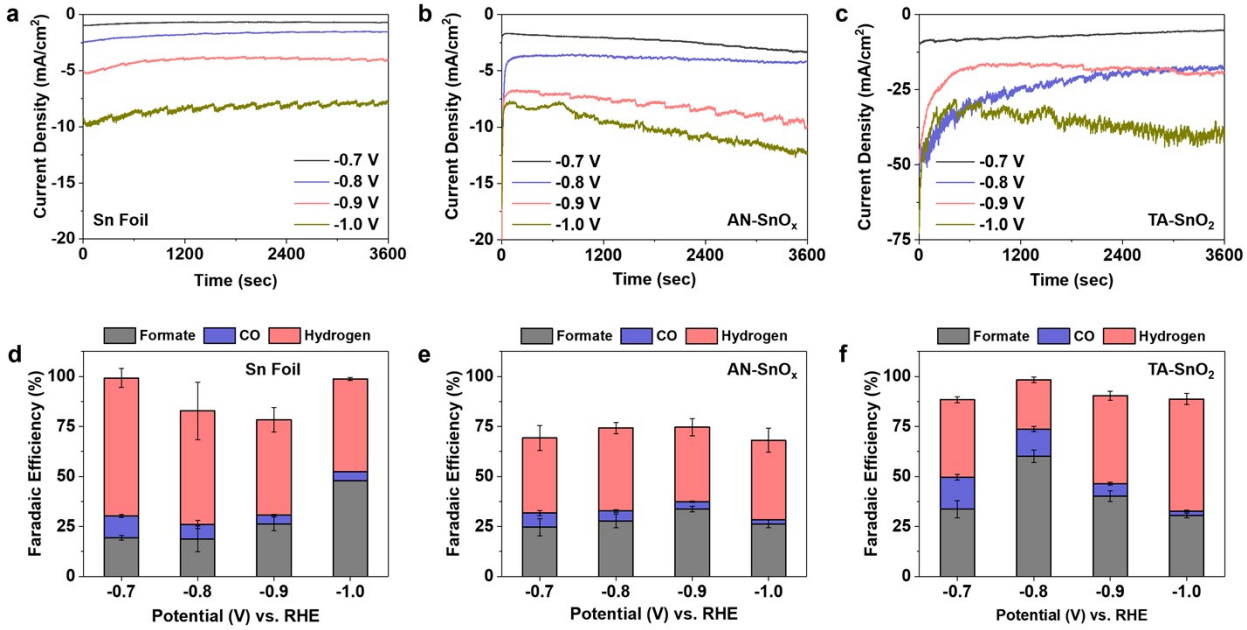

Fig. S7. (a-c) Steady-state CO_2RR measurements of (a) Sn foil, (b) AN-SnO_x, and (c) TA-SnO_2 under various applied potentials. (d-f) Faradaic efficiencies of products for (d) Sn foil, (e) AN-SnO_x, and (f) TA-SnO_2 obtained after the CO_2RR depicted in (a-c), respectively.

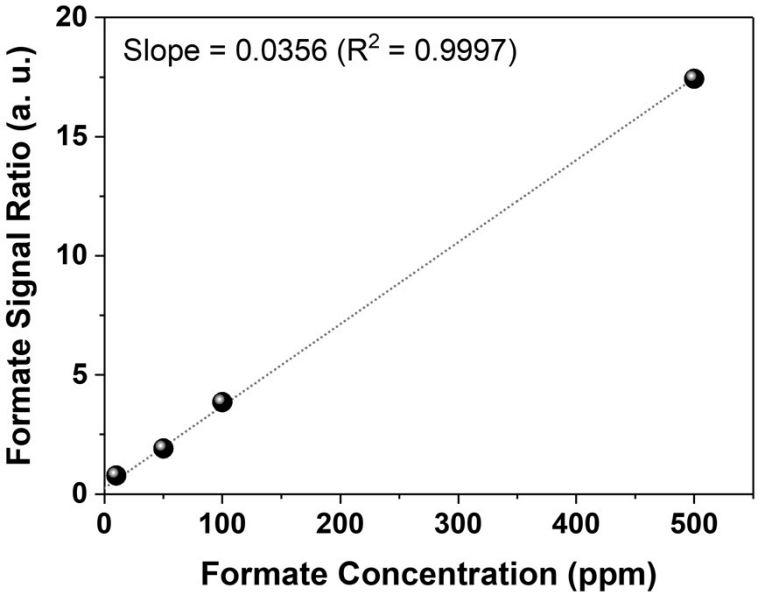

Fig. S8. The calibration curve for the evaluation of formate concentration. The peak area of formate (δ = 8.445) was first modified with respect to reference DSS peak (δ = 0), and the obtained value was calibrated again using the curve above.

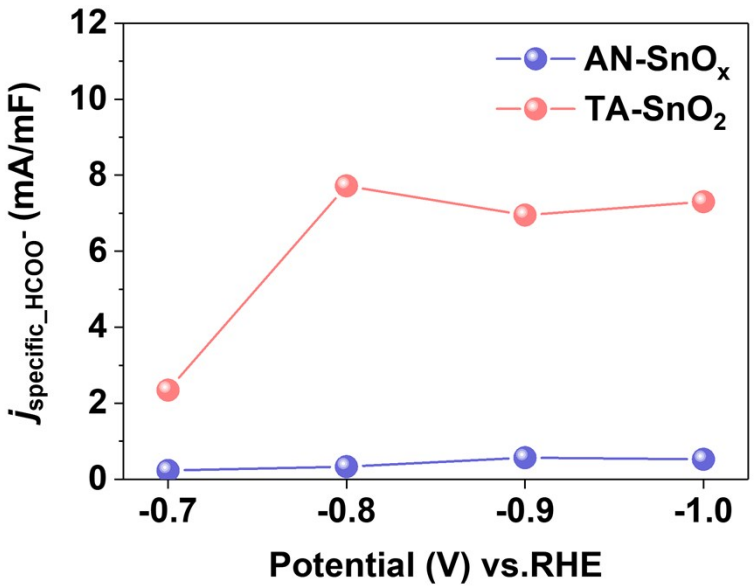

Fig. S9. Comparison between the specific CO_2RR activities of AN-SnO_x and TA-SnO_2 toward formate production by j_{HCOO^-} divided by EDLCs.

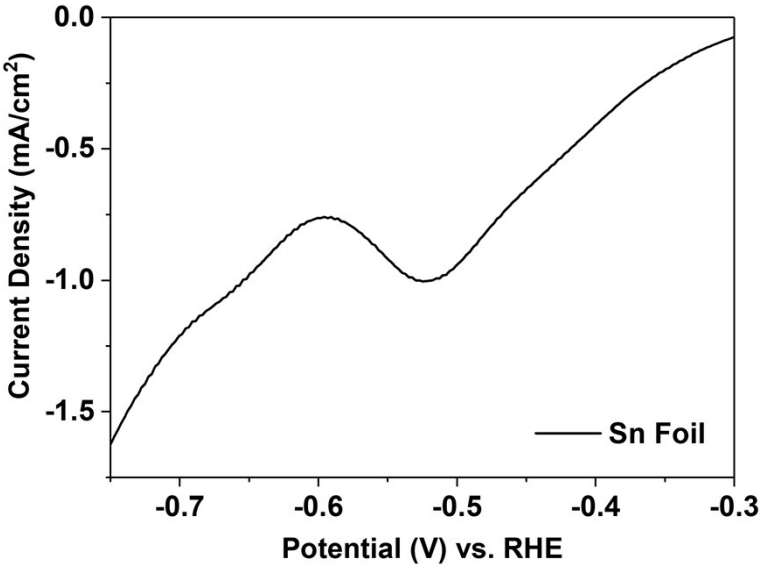

Fig. S10. Magnified version of the CO_2RR curve of bare Sn foil.

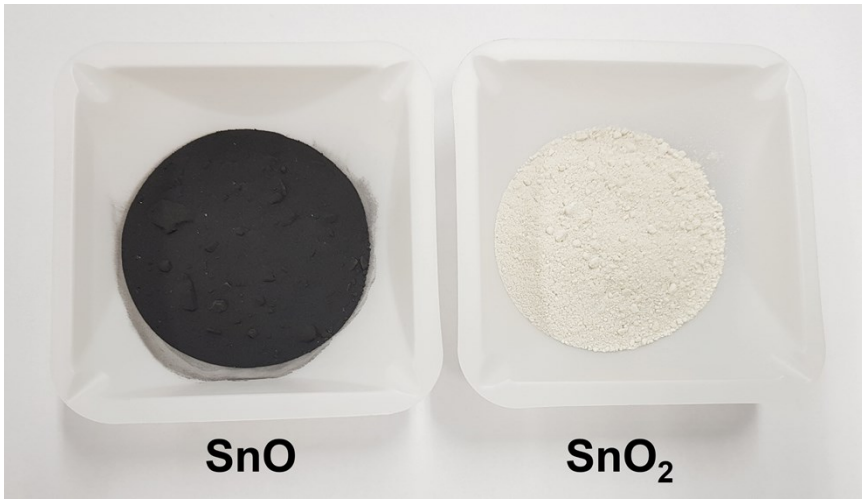

Fig. S11. Digital photograph images of commercial SnO and SnO_2 (from Sigma-Aldrich).

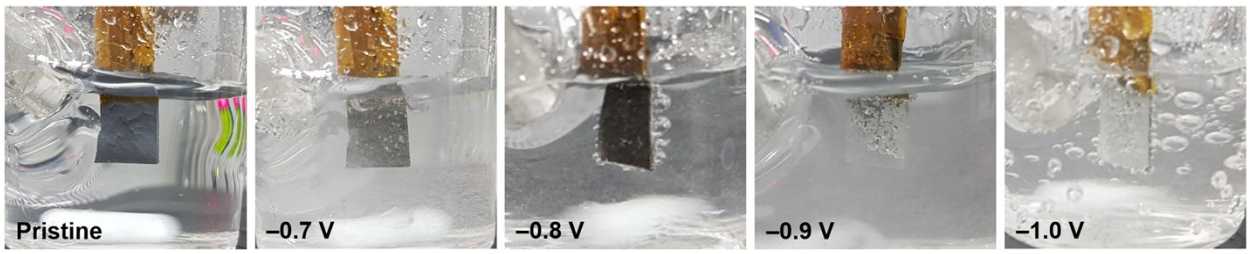

Fig. S12. Digital photograph images of TA-SnO_2 during CO_2RR under various applied potentials.

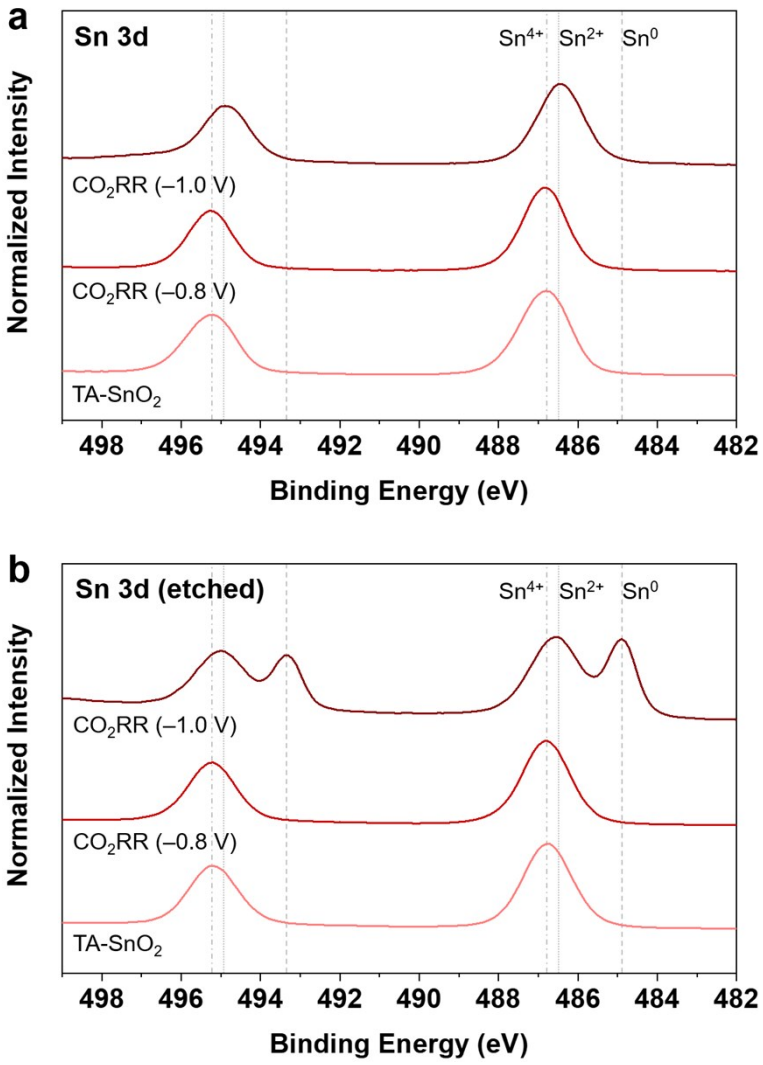

Fig. S13. (a) Bare and (b) surface-etched (1 min Ar-sputtered) XPS Sn 3d spectra before and after CO_2RR.

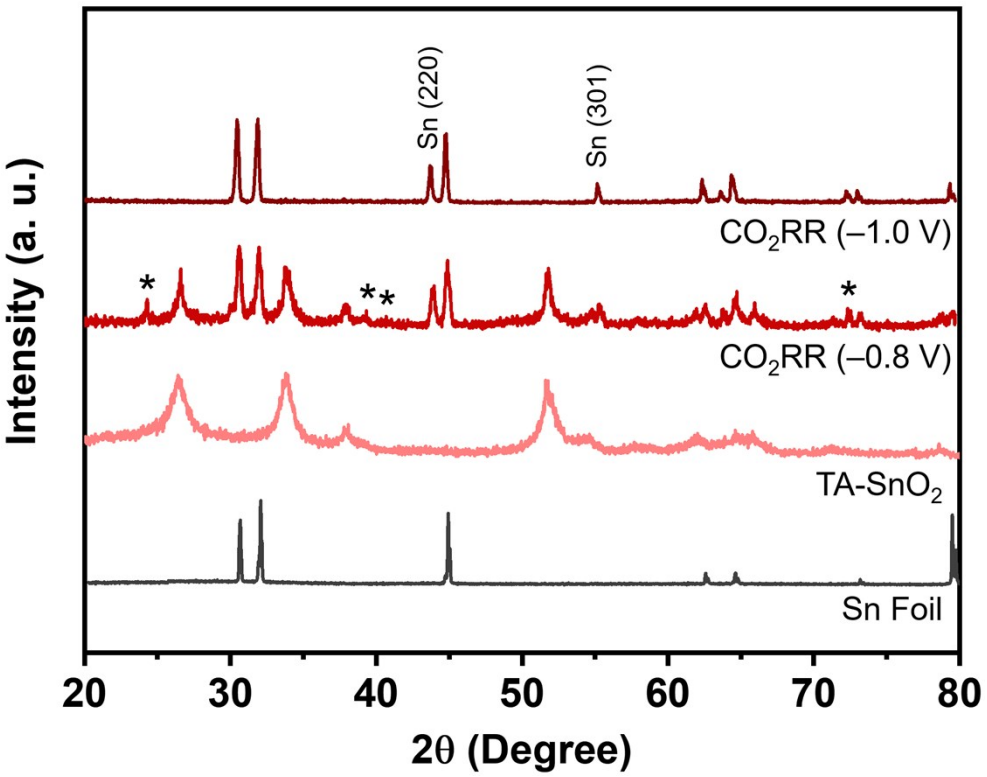

Fig. S14. XRD patterns of TA-SnO_2 before and after CO_2RR at –0.8 V and –1.0 V. The peaks assigned with asterisks are signals from gray Sn (JCPDS #05-0390).

References

S1 R. Daiyan, X. Lu, Y.G. Ng and R. Amal, *Catal. Sci. Technol.*, 2017, **7**, 2542-2550.

S2 D. H. Won, C. H. Choi, J. Chung, M. W. Chung, E. H. Kim and S. I. Woo, *ChemSusChem*, 2015, **8**, 3092-3098.

S3 X. Zheng, Y. Ji, J. Tang, J. Wang, B. Liu, H.-G. Steinrück, K. Lim, Y. Li, M. F. Toney, K. Chan and Y. Cui, *Nat. Catal*., 2019, **2**, 55-61.

S4 W. Luc, C. Collins, S. Wang, H. Xin, K. He, Y. Kang and F. Jiao, *J. Am. Chem. Soc*., 2017, **139**, 1885-1893.

S5 F. Lei, W. Liu, Y. Sun, J. Xu, K. Liu, L. Liang, T. Yao, B. Pan, S. Wei and Y. Xie, *Nat. Commun*., 2016, **7**, 12697.

S6 Y. Chen and M. K. Kanan, *J. Am. Chem. Soc*., 2012, **134**, 1986-1989.

S7 F. Li, L. Chen, M. Xue, T. Williams, Y. Zhang, D. Macfarlane and J. Zhang, *Nano Energy*, 2017, **31**, 270-277.

S8 F. Li, L. Chen, G. P. Knowles, D. R. MacFarlane and L. Zhang, *Angew. Chem. Int. Ed*., 2017, **56**, 505-509.

S9 X. Zheng, P. D. Luna, F. P. D. Arquer, B. Zhang, N. Becknell, M. B. Ross, Y. Li, M. N. Banis, Y. Li, M. Liu, O. Voznyy, C.T. Dinh, T. Zhuang, P. Stadler, Y. Cui, X. Du, P. Yang and E. H. Sargent, *Joule*, 2017, **1**, 794-805.